An Effective Simulation Methodology of Quantum Nanostructures based on Model Order Reduction

Martin Veresko and Ming-Cheng Cheng
Department of Electrical and Computer Engineering
Clarkson University, Potsdam, NY 13699-5720, USA
vereskm@clarkson.edu; mcheng@clarkson.edu

Abstract—**A quantum simulation methodology developed previously based on model order reduction is applied to a 2D nanostructure. The approach is derived from proper orthogonal decomposition that projects the nanostructure from its physical domain onto a function space represented by a finite set of POD modes. Numerical solution data of the wave function are collected from the Schrödinger equation to adapt the variation of the energy band induced by electric fields. The POD modes generated from the data are thus able to account for the variation of electric field. Two different models based on different training methods are explored. Their efficacy and accuracy are investigated.**

Keywords—reduced order model, POD, quantum dots, wave functions, data science

I. INTRODUCTION

Nanostructures have far reaching applications in many scientific and engineering areas. Analysis and design of nanostructures usually rely on numerical simulations of the quantum eigenvalue problems for the nanostructures based on the Schrödinger equation. For example, simulations of quantum dots (QDs) are usually needed for design of QD electronic and photonic devices and they also have many useful applications in medicine, chemistry and material sciences [1-4]. However, large-scale multi-dimensional simulations of the Schrödinger equation often require immense computational power and time, especially in structures with locally non-periodic regions. One typical example is the quantum simulation based on density functional theory (DFT), a quantum mechanical simulation method for calculating electronic structure of atoms, molecules and solids; this method is computationally intensive in large quantum structures, especially with impurities/defects [5-12].

In an attempt to improve the computational efficiency, a quantum simulation methodology [13] was derived from a reduced order learning algorithm based on proper orthogonal decomposition (POD) [14,15]. The approach solves the Schrödinger equation subjected to the energy band variation induced by external electric fields. POD projects the quantum problem from a physical domain onto a functional space represented by a finite set of the basis functions (or POD modes) that are generated via a data training method. The POD quantum model along with domain decomposition was also extended to the quantum element method (QEM) [16,17] that partitions a large quantum domain into subdomain (or elements) to make the approach more flexible and feasible for more complex structure.

The quantum POD modes in previous work [13,16,17] were trained by several sets of wave function (WF) solution data accounting for the variation of electric field along one direction

applied to 1D quantum structures. In this work, the quantum POD simulation methodology is applied to a 2D QD structure whose modes are trained by a few sample data sets of WFs. Instead of using electric fields in many different directions in the 2D domain to train the modes, only electric fields in 2 orthogonal directions are involved. More specifically, in addition to a sample data set at zero field, several WF data sets are collected to adapt the variation of electric field in only one direction, and the other sets in its orthogonal direction. It is found that the trained POD modes are able to predict the WFs influenced by any combination of these 2 orthogonal fields.

Two data training methods are explored in this study: the individual method and the global method. The former trains the modes using the WF data for all quantum states (QSs), which produces one set of POD modes. The latter however trains the modes using WF data in each individual QS, and thus generate a set of POD modes for each state.

II. QUANTUM PROPER ORTHOGONAL DECOMPOSITION

The electron WF is described by the Schrödinger equation,

$$\nabla \cdot \left[\frac{-\hbar}{2m^*} \nabla \psi(\vec{r}) \right] + U(\vec{r}) = E\psi(\vec{r}), \qquad (1)$$

where $\psi(\vec{r})$ is the electron WF, $\hbar$ is the reduced plank constant, m^* is the electron effective mass, $U(\vec{r})$ is the potential energy of the system and E is the QS energy of $\psi(\vec{r})$.

The POD modes $\eta(\vec{r})$ that constitute the POD space are determined via a Fredholm equation [14,15],

$$\int_{\Omega} R(\vec{r}, \vec{r}') \vec{\eta}(\vec{r}) d\vec{r}' = \lambda \vec{\eta}(\vec{r}), \qquad (2)$$

where λ is the eigenvalue associated with the eigenvector $\eta(\vec{r})$ and $R(\vec{r}, \vec{r})$ is a two point correlation tensor given by

$$R(\vec{r}, \vec{r}') = < \vec{\psi}(\vec{r}) \otimes \vec{\psi}(\vec{r}') >. \qquad (3)$$

Once the POD modes are found using the method of snapshots [18,19], the WF can be calculated from a linear combination of these modes,

$$\psi(\vec{r}) = \sum_{j=1}^{M} a_j \eta_j(\vec{r}) \qquad (4)$$

where M is the total number of modes or DoF to represent the WF and a_j are weighting coefficients pertaining to parametric variations of electric fields.

The POD eigenvalues λ_i in (2) represent the mean squared WF captured by the POD modes. Thus, this eigenvalue spectrum reveals information regarding the number of modes needed to

reach a specified accuracy. Given a large enough data set, the theoretical least square (LS) error for a model constructed of M modes is given by

$$Err_{LS,M} = \sqrt{\sum_{i=M+1}^{N_S} \lambda_i / \sum_{i=1}^{N_S} \lambda_i,} \qquad (5)$$

where N_s is the number of parametric variations applied during data collection. This equation only holds if one used identical numerical settings between the data collection and the POD application and if the parametric variations of the application falls within the range of the collected data.

Numerically, the LS error between WFs derived via the quantum POD model and the Schrödinger equation obtained from direct numerical simulation (DNS) is defined as

$$Err_{LS,\psi} = \int_\Omega \left(\psi_{POD,M}(\vec{r}) - \psi_{DNS}(\vec{r}) \right)^2 d\Omega, \qquad (6)$$

where $\psi_{POD,M}$ is the WF produced using the POD model with M modes, while ψ_{DNS} is the corresponding WF solved by DNS.

The equations for a_i are derived by projecting the Schrödinger equation onto the POD modes using the Galerkin projection method. This leads to a Hamiltonian matrix equation in the POD eigenspace [13,16,17],

$$H_\eta \vec{a} = E \vec{a}, \qquad (7)$$

where H_η is given as

$$H_\eta = T_\eta + B_\eta + U_\eta. \qquad (8)$$

In (8), T_η is the interior kinetic energy matrix,

$$T_{\eta i,j} = \int_\Omega \left[\nabla \eta_i(\vec{r}) \cdot \frac{\hbar^2}{2m^*} \nabla \eta_j(\vec{r}) \right] d\Omega, \qquad (9)$$

and B_η is the boundary kinetic energy matrix,

$$B_{\eta i,j} = - \int_S \eta_i(\vec{r}) \frac{\hbar^2}{2m^*} \nabla \eta_j(\vec{r}) dS \qquad (10)$$

and lastly U_η is the potential energy matrix,

$$U_{\eta i,j} = \int_\Omega \eta_i(\vec{r}) U(\vec{r}) \eta_j(\vec{r}) d\Omega. \qquad (11)$$
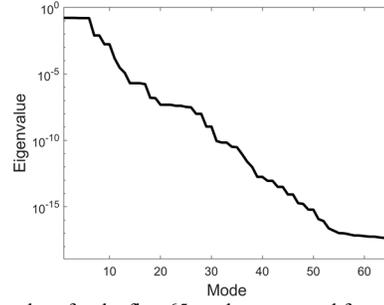
Fig. 1. Eigenvalues for the first 65 modes generated from the global method.

III. APPLICATION OF POD TO A QUANTUM-DOT STRUCTURE

For this study, the Al$_{0.3}$Ga$_{0.7}$As/GaAs heterostructure was selected with the parameters: electron effective mass of $m^* = .0919m_0$ in Al$_{0.3}$Ga$_{0.7}$As and $m^* = .067m_0$ in GaAs, and a conduction band offset at the Al$_{0.3}$Ga$_{0.7}$As/GaAs interface of $\Delta E = 0.24 \, eV$.

To generate POD modes from (2), data of WFs in N_{QS} QSs derived from DNSs of the Schrödinger equation are collected at N_F different applied electric fields. There are different approaches to generate the POD modes and each approach leads to a different POD model. 2 approaches are presented in this work for the 2D QD structure, which are briefly described below.

Global method: This approach performs decomposition given in (2) on the collected WF data in all the selected N_{QS} QSs over the N_F applied electric fields, and thus the total number of the sample data sets is $N_S = N_{QS} \times N_F$. This generates one set of N_S POD modes, and the maximum dimension of the POD Hamiltonian is limited to N_s.

Individual method: Decomposition for this approach is performed on each of QSs separately. This generates a set of POD modes for each QS, and each set is trained by N_F electric field samples in its QS. There are however N_{QS} Hamiltonian matrix equations to solve if WFs in all N_{QS} QSs are needed, and the maximum dimension of the POD Hamiltonian for each QS will equal N_F.
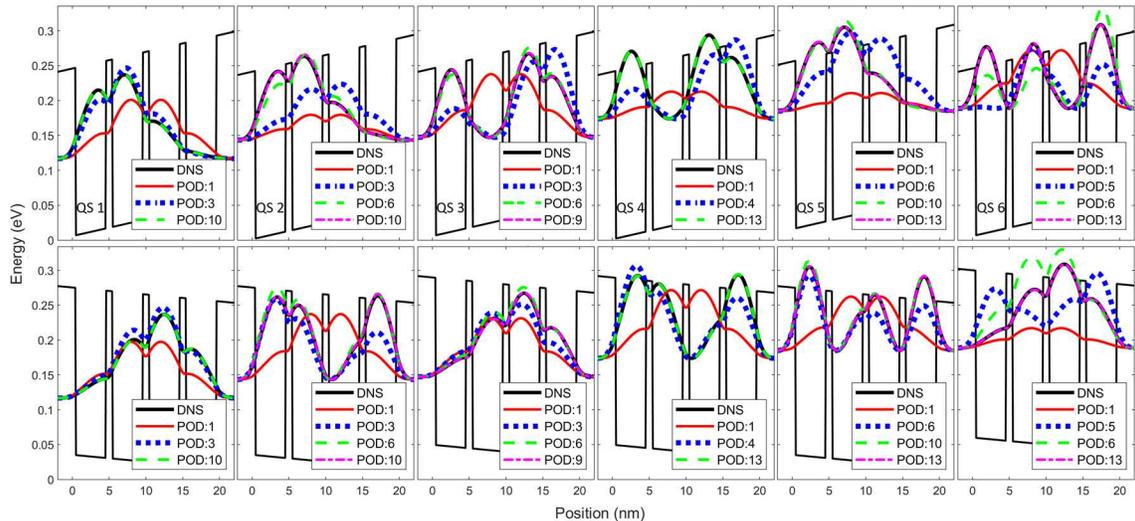
Fig. 2. $|\psi|^2$ in the first 6 QSs in the 2D QD structure predicted by the POD global method compared with the DNS of the Schrödinger equation along the x direction (top row) and the y direction (bottom row). The plotting paths in x and y directions are indicated in the contours given in Fig. 3.
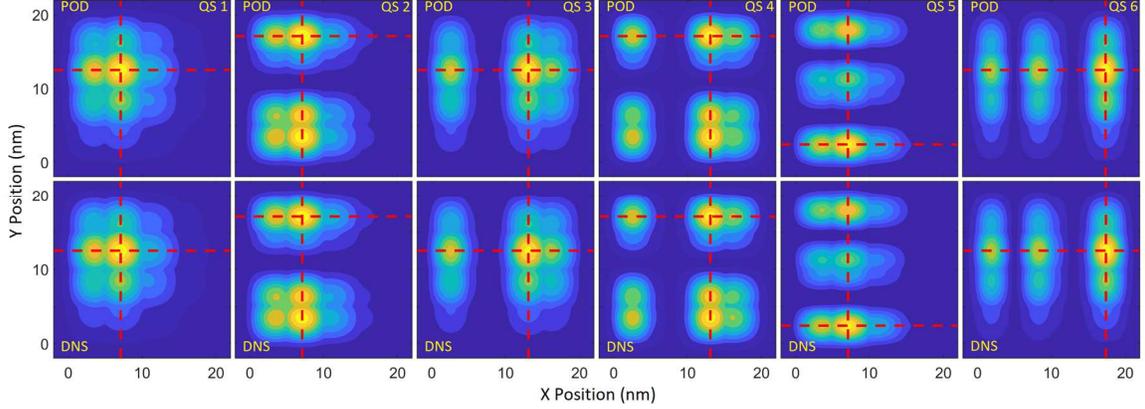
Fig. 3. Contours of $|\psi|^2$ in the QD structure produced via the POD global method (top row) and DNS (bottom row). The red dashed lines reveal the plotting paths for the WFs shown in Fig. 2. For the POD WFs on the top row, 10 modes are included in QSs 1 and 2, 9 modes in QS 3, and 13 modes in QSs 4, 5 and 6.

Both the global and individual methods are examined in a 2D structure with 4×4 QDs and a 2.5nm space on each side of the structure. The QDs, 4nm×4nm in size were each separated by 1nm. DNSs of this QD structure were performed influenced by 16 non-zero electric fields plus an unbiased simulation (electric field = 0); i.e., $N_F = 17$. For each direction ($\hat{x}$, $\hat{y}$, $-\hat{x}$ and $\hat{y}$), 4 electric fields were applied with a maximum value of 25 kV/cm. At each electric field, WFs of the first 6 QSs were collected in the DNS. However, for the demonstrations of both methods, an electric field was applied with a $+\hat{x}$ component of 24kV/cm and a $-\hat{y}$ component of 10kV/cm.

A. Global Method

The eigenvalue of each mode was determined from (2) and its spectrum is plotted as seen in Fig. 1 that indicates the importance of each POD mode. Because only the first 6 QSs are collected, eigenvalues of the first 6 modes are nearly equal, which suggests that for this system Modes 1 through 6 contain essential information on the WFs and cannot be ignored. After Mode 6, the eigenvalue declines rapidly and it drops 3 orders of magnitude from the first to the 10th mode and 4 orders to the 13th mode. It continues decreasing with a similar rate beyond the 13th mode. This suggests that this set of POD modes should offer a good prediction of WFs with 10 modes and a very accurate prediction with 13 modes. Due to the accuracy limited by the number of digits used in numerical calculations, after decreasing by nearly 16 orders of the magnitude from the first mode, the eigenvalue becomes indistinguishable.

The WFs generated via the POD global method are illustrated in Fig. 2 along the paths in the x and y directions shown in the WF contours given in Fig. 3. The first POD mode predicts the average of the WF data used in the training and thus reveals the unbiased solution. The inclusion of more modes gradually improves the accuracy of the POD WF in each state, as shown in Fig. 4, where the LS error of each WF was estimated by (6). The LS error also demonstrates that the POD modes of the global method tend to include more essential information for the lower states, and Fig. 4 shows that an error near or below 1% can be reached for the first 3 QSs with 9 modes. To achieve such an accuracy in QSs 4-6, 13 modes are

needed. Fig. 2 illustrates that, when using 9 or 10 modes for QSs 1-3 and 13 modes for QSs 4-6, the predicted POD WFs are practically identical to the control.
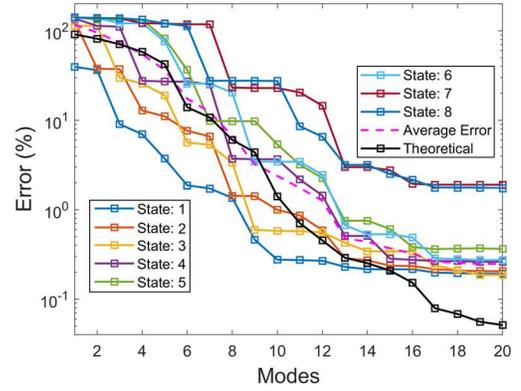
Fig. 4. LS Error for the global method.

TABLE I.   PERCENT DIFFERENCE OF THE QUANTUM STATE ENERGY BETWEEN THE GLOBAL POD METHOD AND DNS

Quantum State	POD Energy (eV)	DNS Energy (eV)	Difference (%)
1	0.116699	0.116778	0.067603
2	0.143238	0.143351	0.07902
3	0.147114	0.147215	0.069048
4	0.173669	0.173806	0.07894
5	0.184776	0.184948	0.092996
6	0.188494	0.188651	0.083426
7	0.215102	0.215293	0.088841
8	0.215259	0.215455	0.091031

Furthermore, Table I reveals that the global method predicts each QS energy accurately. The percent energy difference of each state with respect to the minimum of the potential energy is consistently below 0.1%, even for states 7 and 8 which are not included in the POD mode training. Additionally, the global method has no difficulty computing WFs in degenerate states, such as States 2-3, States 5-6 and States 7-8.
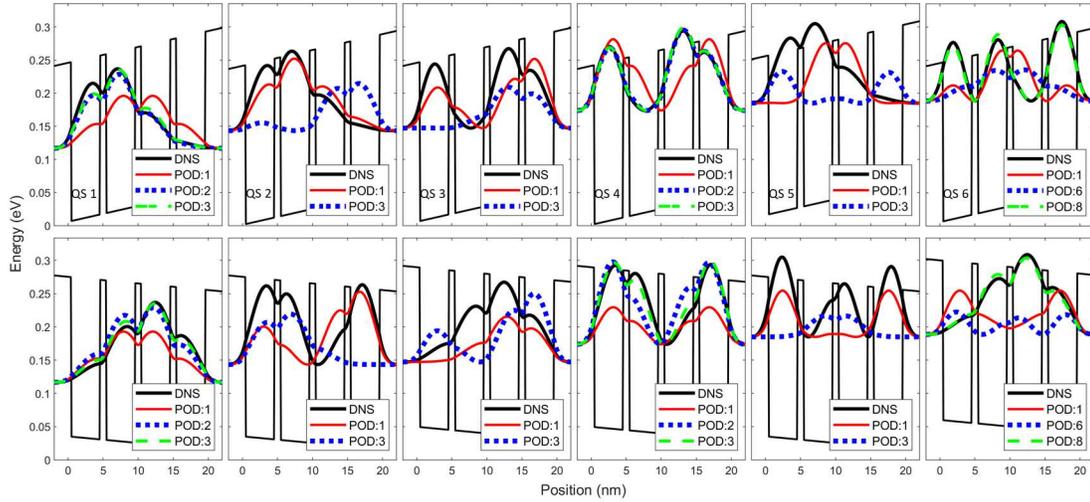
Fig. 5. $|\psi|^2$ in the first 6 QSs in the 2D QD structure predicted by the POD individual method compared with the DNS of the Schrödinger equation along the x direction (top row) and the y direction (bottom row). The plotting paths in x and y directions are indicated in the contours given in Fig. 6.
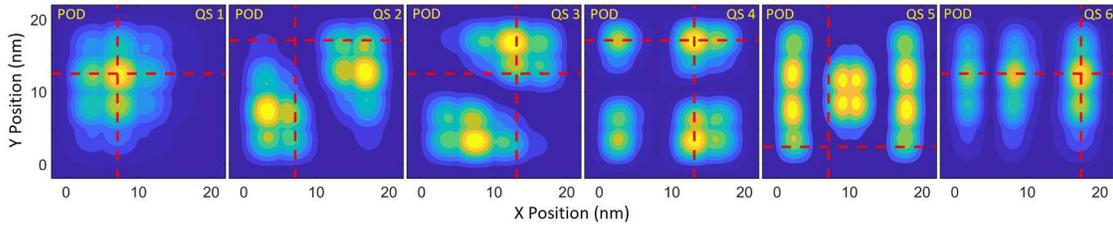
Fig. 6. Contours of $|\psi|^2$ in the QD structure produced via the POD individual method (top row). The red dashed lines reveal the plotting paths for the WFs shown in Fig. 5. For the POD WF contours on the top row, 3 modes are included in QSs 1, 2, 3, 4 and 5, and 8 modes in QS 6. Contours derived from DNS are shown in the bottom row of Fig. 3.
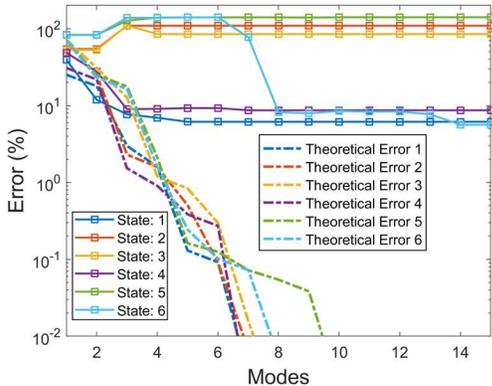
Fig. 7. LS Error for the individual method.

B. Individual Method

Using the same QD structure, the individual POD method was also investigated at the same applied electric field. WFs in QSs 1-6 are illustrated in Fig. 5 along the directions shown in the WF contours given in Fig. 6. As seen clearly, the individual method inaccurately predicts QSs 2, 3 and 5. However, as shown in Fig. 7, the individual method approximately predicts the WFs in QSs 1 and 4 with LS errors near 6.95% and 9%, respectively, using 3 or more modes. In addition, an LS error of 8.2% for QS 6 can be reached with 8 modes and its error reduces to 5.63% with 14 or more modes. One reason why the individual method struggles to accurately predict QSs 2, 3 and 5 is because they are degenerate states. As seen in Table II, QSs 2 and 3 have nearly the same energy, and so do QSs 5 and 6. It is however interesting

to observe in Figs. 5 and 6 that the 6th QS WF is reasonably predicted by the individual method, and its POD energy is actually quite accurate.

TABLE II. Percent Difference of the Quantum State Energy Between the Individual POD Method and DNS

Quantum State	POD Energy (eV)	DNS Energy (eV)	Difference (%)
1	0.116992	0.116778	0.183481
2	0.147012	0.143351	2.521909
3	0.146968	0.147215	0.16791
4	0.173653	0.173806	0.087884
5	0.188662	0.184948	1.987912
6	0.188591	0.188651	0.03168

IV. Conclusion

The quantum POD methodology has been applied to investigate its validity in a QD structure using 2 different methods to generate the POD modes. With relativly few modes, the global method is able to accuratly predict the WFs of the selected QD nanostructure. Even though each data set in the training only experiences one of the 2 orthogonal electric fields, accurate results can be derived from the POD global method responding to a field constructed by these 2 orthognal components. Moreover, it is demonstrated that the global model is able to predict WFs in nearly degenerate states and in the QSs beyond what were included in the training of the POD modes. On the contrastrary, the individual method only offers reasonable accuracy for non-degenerate states and struggles to predict WFs in degenerate states.

REFERENCES

[1] A. A. Andronov, E. P. Dodin, D. I. Zinchenko, "Transport in GaAs/Al$_x$Ga$_{1-x}$As Superlattices with Narrow Minibands: Effects of Interminiband Tunneling," *Semiconductors*, vol. 43, no. 2, pp. 228-235, Feb. 2009, doi: 10.1134/S1063782609020213.

[2] J. Huang, J. L. Jiang, A. Sabeur, "Application of Finite Difference Method in Modeling Quantum Dot Superlattice Silicon Tandem Solar Cell," *AMR* , vol. 898, pp. 249-252, Feb. 2014, doi: 10.4028/www.scientific.net/AMR.898.249.

[3] M. Shen, W. Cao, "Electronic band-structure engineering of GaAs/Al$_x$Ga$_{1-x}$As quantum well superlattices with substructures," *Materials Science and Engineering: B,* vol. 103, no. 2, pp. 122-127, Oct. 2003, doi: 10.1016/S0921-5107(03)00159-4 .

[4] S. A. Tatulian, "From the Wave Equation to Biomolecular Structure and Dynamics," *Trends in Biochemical Sciences*, vol. 43, no. 10, pp. 749-751, Oct. 2018, doi: 10.1016/j.tibs.2018.06.007.

[5] A. J. Cohen, P. Mori-Sánchez, W. Yang, "Insights into Current Limitations of Density Functional Theory," *Science*, vol. 321, no. 5890, pp. 792-794, Aug. 2008, doi: 10.1126/science.1158722.

[6] O. Brea, H. Daver, J. Rebek, F. Himo, "Mechanism(s) of thermal decomposition of N-Nitrosoamides: A density functional theory study," *Tetrahedron*, vol. 75, no. 8, pp. 929-935, Feb. 2019, doi: 10.1016/j.tet.2018.12.054.

[7] S. Hammes-Schiffer, "A conundrum for density functional theory," *Science*, vol. 355, no. 6320, pp. 28-29, Jan. 2017, doi: 10.1126/science.aa13442.

[8] M. F. Ng, M. B. Sullivan, S. W. Tong, P. Wu , "First-Principles Study of Silicon Nanowire Approaching the Bulk Limit," *Nano Lett.*, vol. 11, no. 11, pp. 4794-4799, Nov. 2011, doi: 10.1021/nl2026212.

[9] J. X. Mu, et. Al., "Design, Synthesis, DFT Study and Antifungal Activity of Pyrazolecarboxamide Derivatives," *Molecules*, vol. 21, no. 1, p. 68, Jan. 2016, doi:10.3390/molecules21010068.

[10] M. C. Payne, M. P. Teter, D. C. Allan, T. A. Arias, J. D. Joannopoulos, "Iterative minimization techniques for ab initio total-energy calculations: molecular dynamics and conjugate gradients," *Rev. Modern Physics*, vol. 64, no. 4, pp. 1045-1097, Oct. 1992, doi: 10.1103/RevModPhys.64.1045.

[11] A. Goyal, P. Gorai, H. Peng, S. Lany, V. Stevanović, "A computational framework for automation of point defect calculations," *Comp. Materials Science*, vol. 130, pp. 1-9, Apr. 2017,.

[12] H. S. Zhang, L. Shi, X.-B. Yang, Y.-J. Zhao, K. Xu, L.-W. Wang, "First - Principles Calculations of Quantum Efficiency for Point Defects in Semiconductors: The Example of Yellow Luminance by GaN: CN+ON and GaN:CN," *Advanced Optical Materials*, vol. 5, no. 21, Nov. 2017, doi: 10.1002/adom.201700404.

[13] M. C. Cheng, "A Reduced-Order Presentation of the Schrödinger Equation", *AIP Advances*, vol. 6, No. 9, Sept. 2016, doi: 10.1063/1.4963835.

[14] J. L. Lumley, "The Structure of Inhomogeneous Turbulence," in *Atmospheric Turbulence and Wave Propagation*, A. M. Yaglom and V.I. Tartarski, Ed. Moscow, 1967, pp. 166-178.

[15] J. L. Lumley, *Stochastic Tools in Turbulence.* Mineola, NY, USA: 1970; reprint, Dover publisher, 2007.

[16] M. C. Cheng, "Quantum element method for quantum eigenvalue problems derived from projection-based model order reduction*," AIP Advances*, vol. 10, no. 11, Nov. 2020, doi: 10.1063/5.0018698.

[17] M. C. Cheng, "A Quantum Element Reduced Order Model," in *Int. Conf. Simulation of Semiconductor Processes and Devices (SISPAD)*, Udine, Italy, Sept. 4-6 2019, pp. 1-4.

[18] L. Sirovich, "Turbulence and the dynamics of coherent structures. I - Coherent structures. II - Symmetries and transformations. III - Dynamics and scaling," *Quart. Appl. Math.*, vol. 45, pp. 561–571, Oct. 1987.

[19] W. Jia, B. T. Helenbrook, M. C. Cheng, "Fast Thermal Simulation of FinFET Circuits Based on a Multiblock Reduced-Order Model," *IEEE Trans. CAD ICs. Syst*, vol. 35, pp. 1114–1124, 2016.